38th International Electric Vehicle Symposium and Exhibition (EVS38) Göteborg, Sweden, June 15-18, 2025

Fault-Tolerant DC-DC LLC Converter for Electric Vehicles

Aswathy M. Prince, Ayman Ayad
Schaeffler AG
aswathy.marangattu.prince@vitesco.com ayman.ayad@vitesco.com

Executive Summary

This paper presents a high-efficiency, fault-tolerant LLC DC-DC converter designed for electric vehicles, specifically addressing the requirements of Level 4/5 Autonomous Drive (AD) systems. The converter operates within an input voltage range of 250V to 450V, delivering a 400V/12V output at 1.8kW, with efficiency exceeding 95% during regular operation and above 90% under fault conditions. It complies with the highest Automotive-Safety-Integrity Level (ASIL) standards and offers exceptional reliability, featuring the lowest Failure-In-Time (FIT) rate and maximal availability. To ensure operational continuity, a full-bridge to half-bridge (FB to HB) reconfiguration strategy is implemented to handle high-voltage side faults, alongside soft-switching techniques that reduce losses and electromagnetic interference. The design guarantees a stable low-voltage power supply for safety-critical EV functions. Simulation results and performance analysis validate their robustness, making it a viable solution for next-generation electric vehicle applications.

Keywords: Electric Vehicles, DC-DC, HV/LV, Resonant Converters, Fail-Operation

1 Introduction

Power electronic converters are critical in managing and converting energy within EV powertrains. Recent advancements in wide bandgap (WBG) semiconductor devices, which operate at higher switching frequencies, have greatly enhanced converter performance. However, the high dv/dt and di/dt of WBG devices require additional filter measures for electromagnetic interference (EMI). Addressing these challenges while maintaining high efficiency has become a key focus in EV power electronics research [1]-[4].

Resonant converters, particularly the Inductor-Inductor-Capacitor (LLC) topology, have emerged as a promising solution due to their soft-switching capabilities, reducing losses and mitigating EMI. The LLC converter achieves high efficiency and robust voltage control under varying battery charge states. It minimizes losses with zero-voltage switching (ZVS) and zero-current switching (ZCS). Additionally, its ability to maintain efficiency across wide input ranges makes it ideal for EV applications requiring compatibility with diverse battery voltage levels [5]. Modern electric vehicle auxiliary power systems increasingly adopted advanced DC-DC converter architectures to meet stringent efficiency and power-density requirements. Phase-shifted full-bridge (PSFB) converters are widely implemented in low-voltage DC-DC (LDC) applications, serving dual roles as power conversion units and active harmonic filters. These systems mitigate second-order harmonic currents on DC-link capacitors arising from power factor correction stages during high-voltage battery charging cycles. To ZVS in PSFB primary switches, auxiliary inductive components – discrete inductors or transformer leakage/magnetizing inductances – provide necessary resonant energy for soft-switching transitions across line/load variations [6], [7].

For high-current secondary-side implementations (>200A), current-doubler rectification configurations demonstrate clear advantages by: Halving RMS current stress through parallel inductor paths, enabling ripple current cancellation at output capacitors, facilitating compact magnetic designs through reduced core sizes [6], [7]. While PSFB topologies dominate LDC applications, LLC and LCC resonant converters present compelling alternatives with inherent ZVS for primary switches and ZCS for secondary rectifiers across wide operational ranges [8]-[10]. This intrinsic soft-switching capability reduces switching losses and EMI, particularly beneficial in multi-kilowatt applications. Emerging solutions integrate synchronous rectification (SR) with wide bandgap devices (SiC/GaN) on secondary sides to minimize conduction losses in high-current paths. This technological shift addresses increasing power demands (>2.5kW) while maintaining compact form factors through: Reduced thermal management requirements, higher switching frequency operation, improved transient response characteristics [7], [8].

An LLC converter with a reconfigurable rectifier has been proposed for wide output voltage range applications in [11]. This topology includes two sub-rectifiers (sub-R) in parallel, and it can be expanded by adding more sub-rectifiers for ultra-wide voltage range applications. It uses frequency modulation (FM), while phase-shift (PS) control is applied for smooth transitions between rectifier modes. However, this topology requires either two transformers or a multi-winding transformer, unlike conventional LLC converters. Another topology [12] with a similar design objective features an adjustable turns ratio, where the transformer's secondary winding includes an extra tap, allowing the secondary turns to switch among three combinations: n2, n3, and n2 + n3. With four modes of operation, the voltage gain range is reduced by four times while keeping the switching frequency close to resonance. Experimental results achieved 90%–97.5% efficiency for a 60 V–450 V output voltage setup.

This paper introduces a standalone LLC converter featuring a voltage doubler rectifier on the secondary side, designed to deliver high-reliability power for safety-critical systems. Section 2 details the stand-alone fault-tolerant FB LLC converter's operating principle and control strategy. Simulation results are discussed in Section 3, followed by a comprehensive performance analysis in Section 4, and concluding remarks are provided in Section 5.

2 Working Principle

Under permanent failure conditions, SiC switches can experience open-circuit (OC) or short-circuit (SC) faults. OC faults are less critical for voltage source converters like the LLC as power transfer is naturally interrupted. In contrast, SC faults pose a significant risk, as they can cause severe damage to the power converter and, more critically, to the battery pack through overheating or thermal runaway. While redundant converters or auxiliary batteries are commonly employed to sustain auxiliary systems during failures, this work introduces a standalone fault-tolerant mechanism that eliminates the need for additional hardware [13].

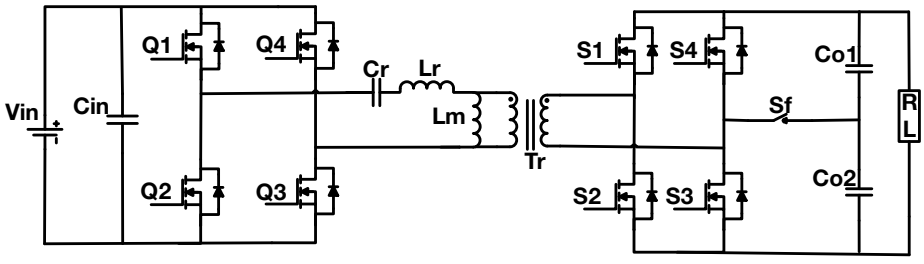

Figure 1: Fault-Tolerant LLC converter

2.1 Fault-Tolerant LLC converter topology

The fault-tolerant LLC converter, illustrated in Fig. 1, primary side operates in FB mode under normal conditions and transitions to HB mode in the event of a SC fault in a semiconductor. However, this results in the output voltage being halved, which is undesirable for auxiliary load requirements. To address this, a modification is introduced on the secondary side, incorporating two split capacitors and an additional switch (Sf). Sf can be bidirectional back-to-back MOSFETs. This setup allows one side of the high-

frequency transformer's secondary winding to connect directly to the capacitor midpoint, forming a voltage doubler rectifier (VDR). This approach ensures the converter maintains its output voltage and critical functionality after a fault [14].

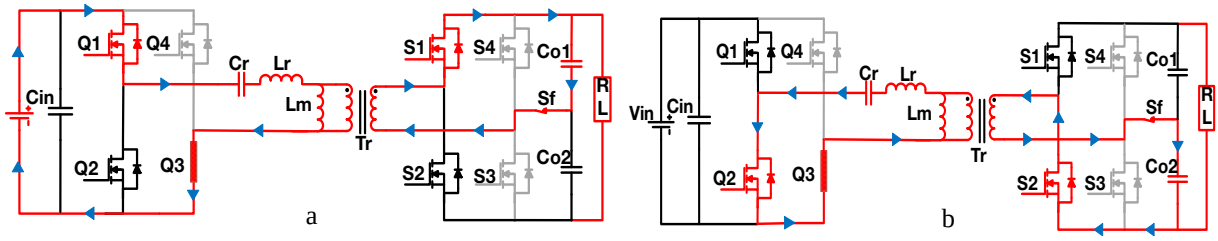

Figure 2: Fault-case: direction of current flow (a) during positive and (b) excitation voltage on the resonant network

2.2 Operation under fault

During normal operation, the rectifier functions as a standard FB rectifier with switch Sf open. In the event of a fault, switch Sf is activated, bypassing the leg formed by Si MOSFETs S3 and S4. This configuration connects the bottom side of the secondary winding to the midpoint of capacitors Co1 and Co2, as illustrated in Fig. 2. As a result, the circuit transitions to a VDR, producing an output voltage that is twice the normal value. To explain the converter's reconfiguration, a hypothetical fault scenario is considered where switch Q3 suffers a permanent SC fault. This causes the FB to produce an asymmetric waveform, necessitating the following steps to restore operation:

- Switch Q4 is permanently open-circuited, while Q3, now short-circuited, is utilized as part of the current commutation path.
- Switches Q1 and Q2 are controlled with complementary PWM signals, forming an HB circuit. Simultaneously, switch Sf is activated, allowing the output stage to operate as a VDR.

This reconfiguration ensures that the output voltage remains stable and maintains the converter's functionality despite the fault. While primarily analyzed for SC faults, the reconfiguration scheme also applies to OC faults.

2.3 Control System Architecture and Stability Optimization

The control framework of power converters ensures operational precision and stability by dynamically regulating system behavior. In standard operating regimes, the proposed converter architecture mirrors the performance characteristics of conventional LLC resonant topologies, enabling compatibility with frequency-modulated pulse-width modulation (PWM) strategies. These methods leverage voltage-controlled oscillators (VCOs) to generate switching signals, maintaining alignment with established resonant converter control paradigms.

2.3.1 Small-Signal Modeling for Transfer Function Extraction

A systematic approach to digital controller design involves deriving the control-to-output transfer function through simulated small-signal analysis. The methodology comprises three stages:

- Perturbation Injection: A low-amplitude sinusoidal signal, imperceptible to nominal operation, is introduced across a swept frequency spectrum in open-loop configuration.
- Frequency Response Characterization: Output modulation patterns are analyzed to quantify gain and phase relationships, forming empirical Bode plot data.
- Model Approximation: The frequency-domain response is mathematically represented as a transfer function, capturing the plant dynamics for controller synthesis.

2.3.2 **Closed-Loop Controller Implementation**

The derived transfer function serves as the foundation for constructing a proportional-integral (PI) compensator within a digital control architecture. This closed-loop configuration enables:

- Real-time output voltage regulation via feedback mechanisms
- Attenuation of load-induced disturbances
- Enhanced transient recovery performance during operational mode transitions

The integration of simulation-based frequency analysis with controller optimization provides a replicable framework for stabilizing resonant power conversion systems while minimizing design iteration cycles. This approach balances theoretical rigor with practical implementation requirements, ensuring robust performance across variable operating conditions. Traditional PI controllers employed in LLC converters frequently exhibit inadequate regulation when subjected to broad input voltage variations and rapid load fluctuations. This limitation stems from the use of fixed gain parameters, which are often insufficient to accommodate the dynamic disturbances encountered during operation. To overcome this constraint, a variable gain control approach is adopted. By conducting small-signal analysis under a range of load conditions, optimal gain values corresponding to different per unit (p.u.) load scenarios are identified. Gain parameters are then systematically tuned using a PI controller optimization process to ensure optimal regulation performance, targeting at least a 20 dB gain margin, a phase margin exceeding 60 degrees, and consistent settling times across all cases. The results of this analysis indicate that the proportional gain (Kp) can remain constant, whereas the integral gain (Ki) must be adjusted in response to load changes. This adaptive method ensures robust regulation and stability across a wide spectrum of operating conditions.

2.3.3 **Control Strategy**

The control strategy for the stand-alone fault-tolerant power converter is comprehensively illustrated in Fig. 3, reflecting a multi-state operational protocol designed to ensure both robust performance and resilience to faults. Upon system initialization, a controlled soft-start mechanism is triggered to gradually energize the converter, effectively mitigating inrush currents and stabilizing the primary power stage. This process is immediately followed by a parallel diagnostic phase, which continuously interfaces with the fault detection subsystem to rigorously monitor the integrity of the switching devices in real time. In the absence of detected abnormalities, the controller advances to FB operational mode. Here, a proportional-integral (PI) controller, enhanced by a preconfigured lookup table referencing both output voltage and normalized load, orchestrates the precise generation of PWM signals essential for efficient LLC converter operation. This hybrid control approach dynamically adjusts switching parameters, optimizing system efficiency across varying load conditions and ensuring stable output performance. If a fault is detected, the controller transitions into a specific state aligned with the nature of the anomaly: overcurrent (OI), single-switch short circuit (SC1), multiple-switch short circuit (SCM), single-switch open circuit (OC1), or multiple-switch open circuit (OCM). Upon fault recognition, all gate signals are immediately disabled, and the system re-engages the soft-start routine to reassess the fault status and determine the appropriate recovery path. If the fault persists, the controller executes targeted mitigation actions based on the identified state:

- For OI, the system restricts load current and verifies whether the anomaly has been resolved; if not, the state escalates to SC1 or SCM, depending on the number of affected switches.

- For SCM or OCM, the converter is rendered inoperative, necessitating the activation of the auxiliary battery to maintain system continuity.
- For SC1, the controller initiates a transition to HB reconfiguration, selecting the appropriate switches for HB operation as determined by the corresponding logic table. The same approach is applied to OC1.

The logic governing the transition between FB and HB modes is detailed in Table 1. Transitions from FB to HB mode are always accompanied by an additional soft-start cycle, specifically implemented to suppress output voltage overshoot that may result from abrupt changes in inductive current.

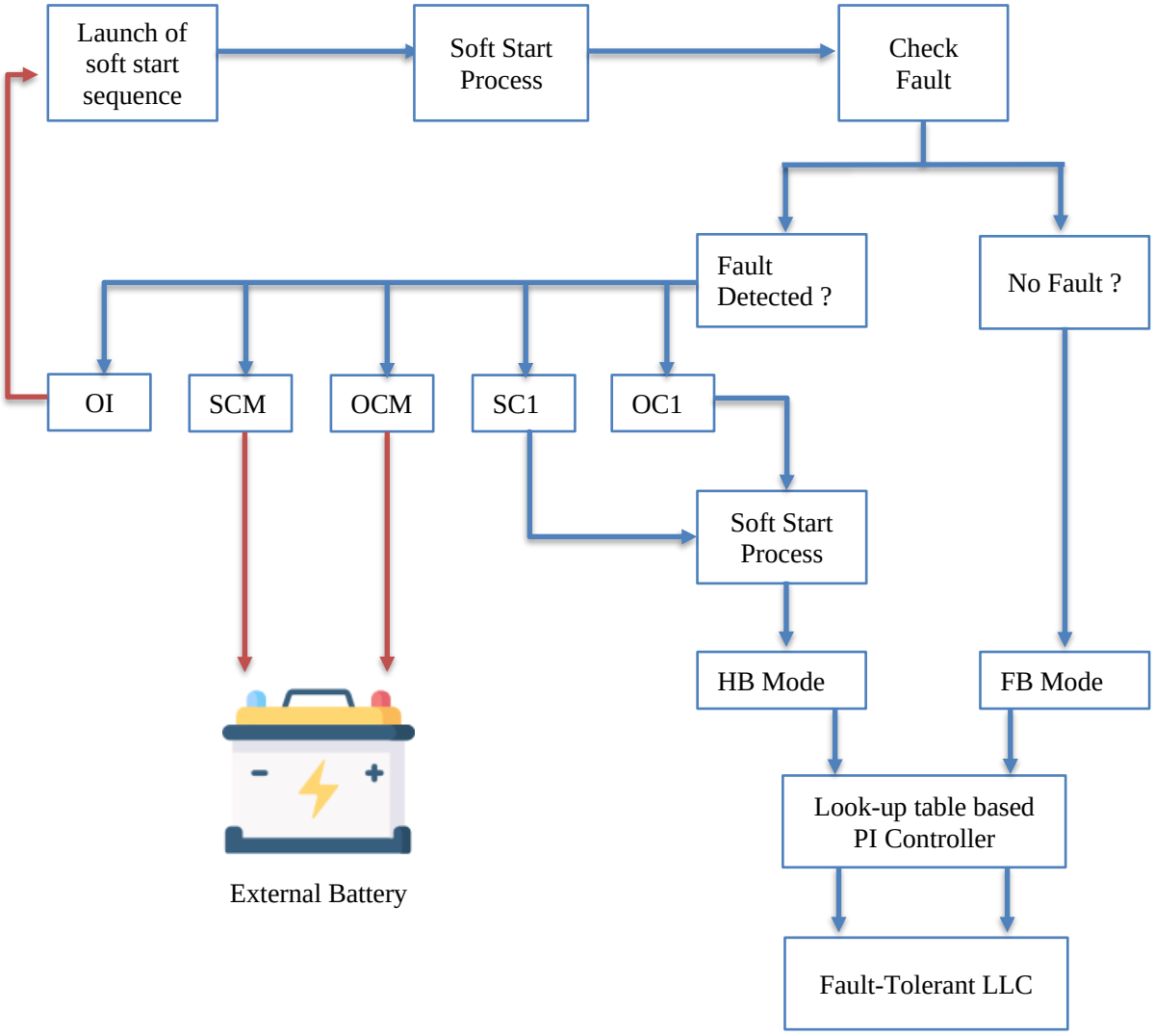

Figure 3: Control logic of the stand-alone fault-tolerant LLC converter

Table 1: Switching states for the reconfiguration scheme

Faulty Device	Q1	Q2	Q3	Q4
Q1	SC	OFF	switching	switching
Q2	OFF	SC	switching	switching
Q3	switching	switching	SC	OFF
Q4	switching	switching	OFF	SC
Q1	OC	ON	switching	switching
Q2	ON	OC	switching	switching
Q3	switching	switching	OC	ON
Q4	switching	switching	ON	OC

Table 2: Design parameters

Parameters	Value
Input Voltage Range	250 V - 450 V
Output Voltage	12 V
Output Power	1.8 kW
Resonant Frequency	200 kHz
Switching Frequency Range	97 kHz - 340 kHz
Inductance Ratio	6.62
Quality Factor	0.31
Magnetizing Inductance	93.5 µH
Resonant Tank Inductance	16.65 µH
Resonant Tank Capacitance	38.1nF
Transformer Turns Ratio	32

The logic governing the transition between FB and HB modes is detailed in Table 1. Transitions from FB to HB mode are always accompanied by an additional soft-start cycle, specifically implemented to suppress output voltage overshoot that may result from abrupt changes in inductive current. This phased reactivation ensures smooth topology reconfiguration and verifies fault clearance status between operational states. The entire architecture's layered fault response, combining hardware-protected shutdowns with software-driven recovery attempts, is engineered to achieve high reliability and maintain critical power delivery even under adverse conditions.

3 Simulation Results and Discussion

Table 2 represents the design parameters for the standalone fault-tolerant FB LLC converter, detailing the critical resonant tank values including magnetizing inductance (Lm) of 93 µH, resonant inductance (Lr) of 16 µH, and resonant capacitance (Cr) of 38 nF. The transformer turns ratio (Np/Ns) of 32 enables appropriate voltage conversion while handling the substantial 1800W power requirement. The effective AC resistance (Rac) of 67 Ω reflects the load characteristics, while the quality factor (Q) of 0.313 and inductance ratio (m) of 6.62 ensure the converter can maintain soft-switching across its wide input voltage range (250V-450V). These carefully selected parameters enable the converter to deliver a regulated 12V output at 150A even when transitioning between operational modes during fault conditions, making it particularly suitable for critical applications requiring uninterrupted power delivery despite potential semiconductor failures.

Figure 4 represents the LLC converter gain function for the designed standalone fault-tolerant FB LLC converter. The gain curve illustrates the voltage transfer characteristics across the operational frequency spectrum, highlighting the converter's ability to maintain regulated output despite input variations. This fault-tolerant architecture can reconfigure from FB to HB operation when semiconductor failures occur, ensuring continued power delivery under abnormal conditions. The blue curve demonstrates the resonant behavior with a pronounced peak gain occurring at lower normalized frequencies, where the converter achieves its maximum voltage gain of 1.540 (Mmax, indicated by the red horizontal line). As the normalized frequency increases beyond resonance, the gain gradually decreases, reaching the minimum gain value of 0.856 (Mmin, green horizontal line) at higher frequencies. The optimal operating region (Mopt) is defined by the yellow dashed vertical lines, indicating the normalized frequency band for maximum efficiency and stability. This frequency modulation approach enables the converter to operate from 97 kHz (at f/fr = 0.485) to 340 kHz (at f/fr = 1.70), with a nominal frequency of 200 kHz.

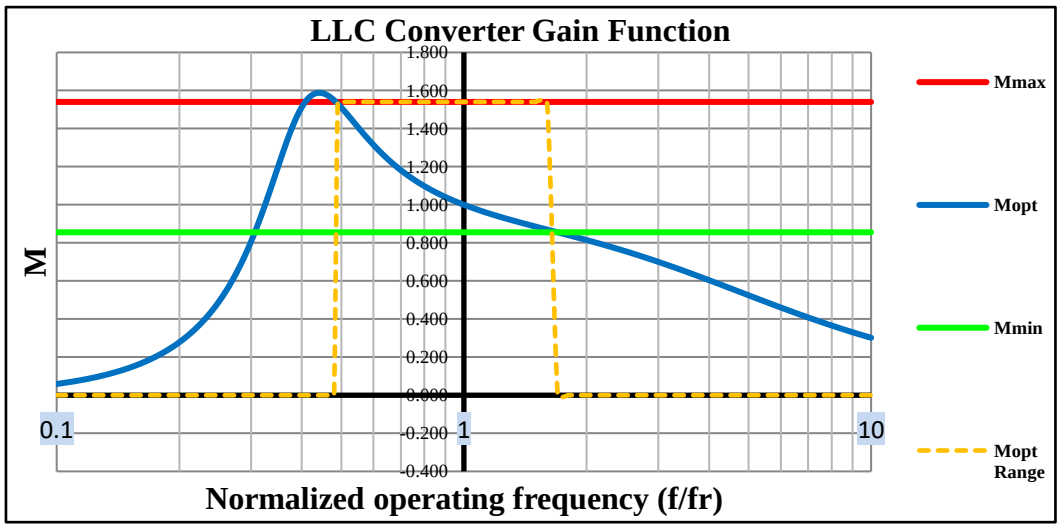

Figure 4: Gain vs. Normalized Frequency for Q = 0.31

To evaluate the fault-tolerant capability of the proposed converter, a SC fault was introduced on the high-voltage side switch (Q3) at 50 ms within a 100 ms simulation period. The switching devices Q1, Q3, Q2, and Q4 operate under complementary pulse-width modulation control signals maintaining a precise 50% duty ratio. This configuration facilitates comprehensive fault-tolerance evaluation, wherein the primary research objective involves analyzing operational continuity when component failures occur. The investigation methodically

examines fault propagation effects throughout both the primary switching network and the secondary rectification stage of the standalone fault-tolerant LLC resonant converter. Particular emphasis is placed on evaluating the effectiveness of the secondary-side rectifier reconfiguration methodology, which maintains power delivery despite primary-side semiconductor failures. For implementation purposes, the system utilizes a control architecture based on pre-calculated lookup tables for frequency modulation and gain adjustment. This control framework was developed using MATLAB Simulink environment, while circuit-level performance verification and thermal analysis were conducted through PLECS simulation platform to validate system behavior under both normal operation and fault conditions. Figure 5 (a) and (b) display the waveforms on the primary side of the fault-tolerant LLC topologies before and after the SC fault at Q3 In the event of a fault, the converter's primary side is reconfigured from FB to HB operation by keeping switch Q4 permanently open and imposing a continuous short-circuit condition on switch Q3. Before any fault occurs, the converter operates in FB mode, characterized by bidirectional voltage across the primary side; however, following the fault, this voltage becomes unidirectional. Notably, the peak-to-peak voltage across the resonant capacitor (Vc) increases by a factor of 1.7 compared to its original value, thereby enabling the converter to maintain operation despite the fault. Although the magnetizing current (Im) is reduced to half its pre-fault magnitude, the resonant current (Ir), which maintains its sinusoidal waveform, remains nearly unchanged. At the conclusion of each switching half-cycle, the current through the resonant inductor aligns with the magnetizing current, while the rectifier current drops to zero. Importantly, ZVS is achieved during the dead-time interval whenever the resonant current equals the magnetizing current, ensuring efficient and reliable commutation even under fault-induced operational constraints.

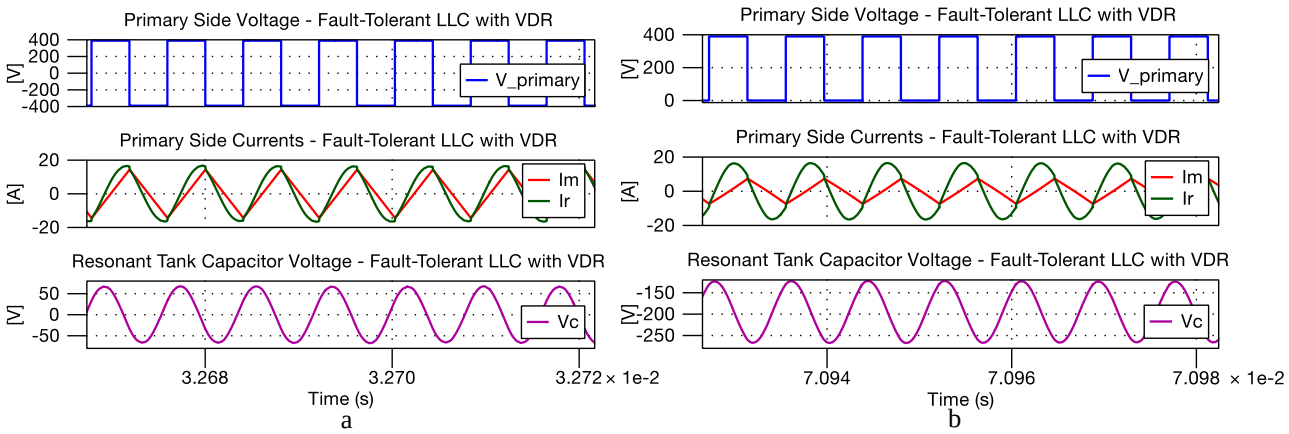

Figure 5: (i) Primary side voltage (Vprimary), (ii) magnetizing inductor current (Im) and resonant tank inductor current (Ir), and (iii) resonant tank capacitor voltage (Vc) (a) before the fault, and (b) after the fault.

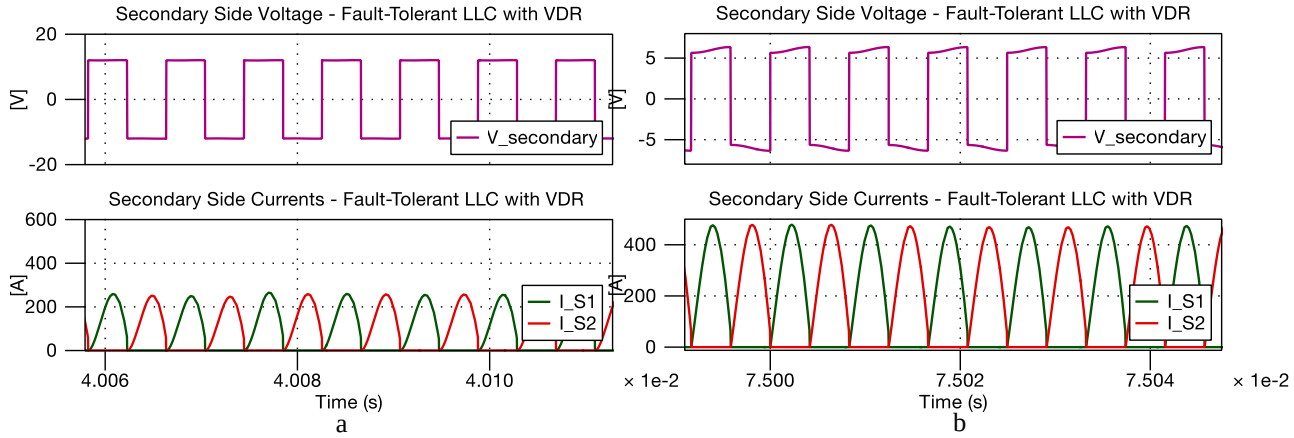

Fig. 6: Secondary side diode currents of fault-tolerant LLC with VDR (a) before the fault and (b) after the fault

Fig. 6(a) and (b) depict the secondary-side switch current dynamics of the fault-tolerant LLC converter incorporating a VDR. The resonant operation inherent to the topology ensures ZCS at the secondary side, effectively eradicating reverse recovery losses in diodes and substantially lowering overall switching losses. Analysis of the waveforms reveals that under fault conditions, the secondary-side currents exhibit a twofold

amplification, specifically, currents I_S1 and I_S2 scale to 2 I_S1 and 2 I_S2, respectively, regardless of whether synchronous or passive rectification is employed, while the secondary side voltage (V_sec) reduces to half. This current doubling arises from the VDR's reconfiguration during fault mitigation, which compensates for reduced voltage gain by redistributing power through active switches. Despite increased conduction losses from elevated current magnitudes, the sinusoidal current profiles inherent to LLC operation preserve ZCS commutation, ensuring sustained efficiency. VDR architecture counterbalances these effects through split-capacitor voltage balancing and adaptive rectifier control, maintaining stable output regulation without compromising the converter's fault-resilient performance.

Key waveforms for varying input voltages minimum (250 V), nominal (385 V), and maximum (450 V) are presented in Figures 7 (a), (b), and (c), respectively. Each figure includes the input voltage waveform, a load current of approximately 150 A, and an output voltage of 12 V. During the reconfiguration from FB to HB mode following fault detection, the fault-tolerant time interval (FTTI) for an input of 250 V was 0.3 ms, with output voltage (Vomax = 12.5 V, Vomin = 10.3 V) and current (Iomin = 130 A, Iomax = 156 A). For the nominal input of 385 V, the FTTI was 0.2 ms, maintaining Vomax and Vomin at 12.5 V and 10.3 V, respectively, and current between Iomin = 130 A and Iomax = 156 A. At the maximum input voltage of 450 V, no overshoots were observed, with Vomin at 10 V, Iomin at 122 A, and an FTTI of 0.2 ms. Table 3 represents EBN_CU for 12 V systems where EBN_CU: Conditions of Use of the SR (Safety Relevant)-Loads for the Energiebordnetz or Electrical Power Supply System and FSR: Functional Safety Requirement.

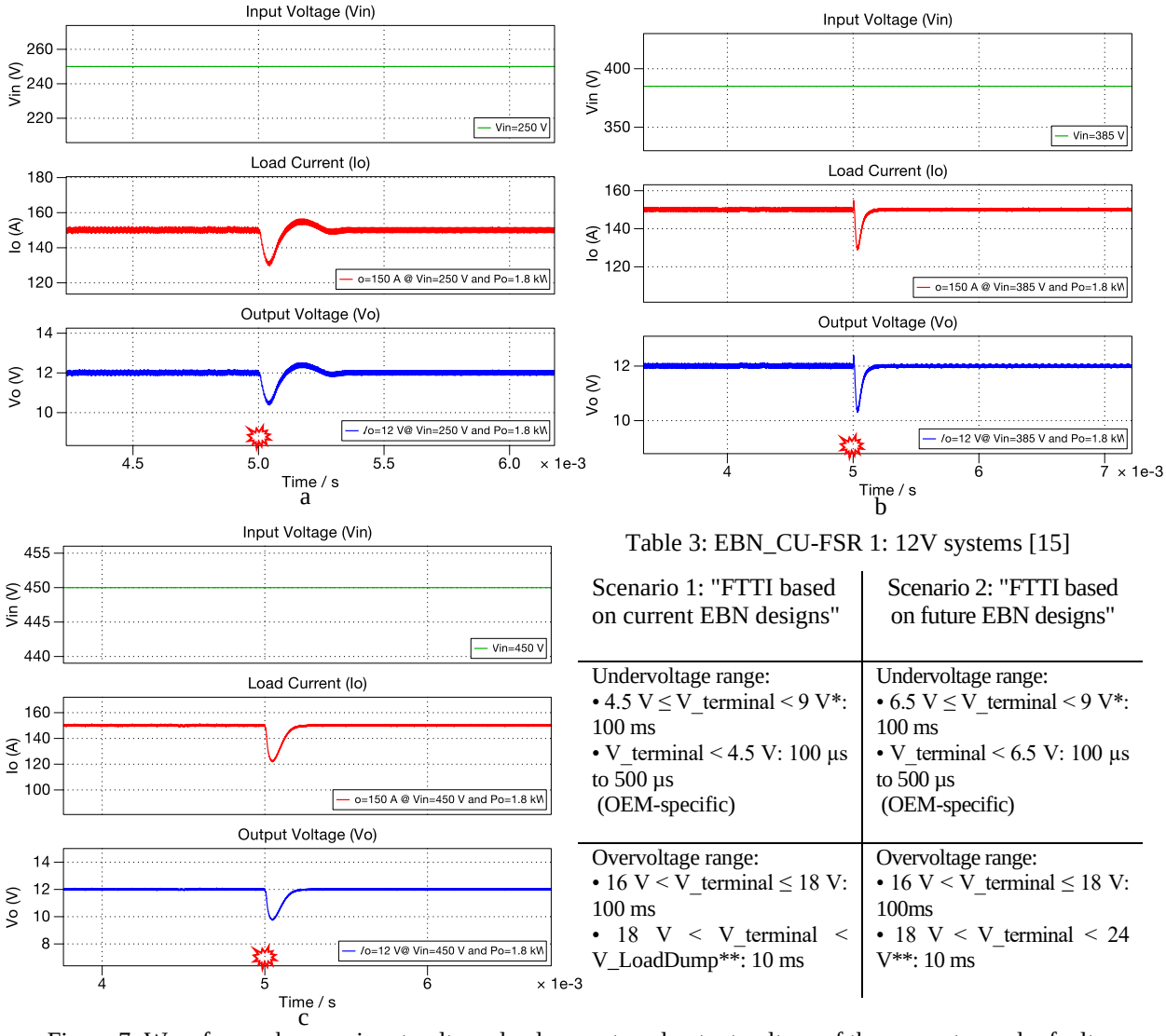

Table 3: EBN_CU-FSR 1: 12V systems [15]

Scenario 1: "FTTI based on current EBN designs"	Scenario 2: "FTTI based on future EBN designs"
Undervoltage range: • 4.5 V ≤ V_terminal < 9 V*: 100 ms • V_terminal < 4.5 V: 100 µs to 500 µs (OEM-specific)	Undervoltage range: • 6.5 V ≤ V_terminal < 9 V*: 100 ms • V_terminal < 6.5 V: 100 µs to 500 µs (OEM-specific)
Overvoltage range: • 16 V < V_terminal ≤ 18 V: 100 ms • 18 V < V_terminal < V_LoadDump**: 10 ms	Overvoltage range: • 16 V < V_terminal ≤ 18 V: 100ms • 18 V < V_terminal < 24 V**: 10 ms

Figure 7: Waveforms showing input voltage, load current, and output voltage of the converter under fault conditions and reconfiguration for (a) 250 V, (b) 385 V, and (c) 450 V input voltages.

4 Performance Analysis

A comprehensive market survey was conducted to identify suitable SiC MOSFETs for both high-voltage (HV, 650 V) and low-voltage (LV, 60 V) applications relevant to automotive-grade fault-tolerant power converters. Following the selection process, detailed thermal modeling of the shortlisted devices was carried out using PLECS to evaluate their thermal behavior and loss characteristics under normal and faulty operating conditions. To optimize converter efficiency, various combinations of HV and LV switches were analyzed, aiming to minimize conduction and switching losses. From an initial pool of 24 HV-side SiC MOSFETs and 18 LV-side MOSFETs from multiple vendors, the top five candidates from each category were shortlisted based on their superior loss performance. Subsequently, multiple HV-LV switch pairings were evaluated to identify combinations yielding the lowest total losses, thereby enhancing the overall efficiency of the standalone fault-tolerant LLC converter. Table 4 summarizes the best-performing selected HV and LV switches with the lowest losses, and Table 5 shows the five most optimal HV and LV switch pairings determined through a detailed loss analysis.

Table 4: Best 5 HV and LV switches

HV Switches	*Switch Losses (W)*
A	5.25
B	9.15
C	7.26
D	7.56
E	7.57
LV Switches	*Switch Losses (W)*
I	33.73
II	34.54
III	47.63
IV	65.07
V	72.39

Table 5: Optimised HV and LV switch combinations

Switch Combination	HV Switches	LV Switches
Variant 1	A	I
Variant 2	B	II
Variant 3	C	III
Variant 4	D	IV
Variant 5	E	V

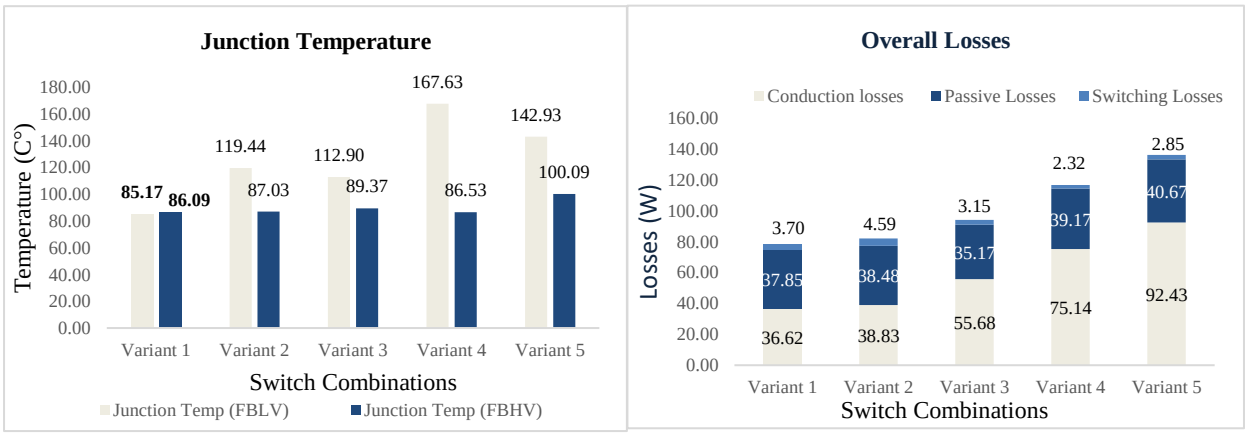

Figure 8 (a): Comparative analysis of junction temperatures for selected switch variants, (b) Breakdown of overall power losses across optimized switch variants in fault-tolerant LLC converter

Fig. 8(a) illustrates the junction temperature profiles of both FB low-voltage (FBLV) and FB high-voltage (FBHV) switches across five optimized switching device combinations. The thermal performance was evaluated under identical operating conditions using a detailed electro-thermal simulation in PLECS. Among the evaluated variants, Variant 1 demonstrates the most thermally balanced operation, with minimal temperature differential between LV and HV switches. In contrast, Variant 4 exhibits the highest thermal stress on the HV side, peaking at 167.63°C, indicating potential reliability concerns under sustained load. This analysis is instrumental in correlating device selection with thermal stability, aiding in the design of a robust,

fault-tolerant LLC converter architecture. thermal and efficiency trade-offs inherent in component-level selection for fault-tolerant power architectures. Figure 8(b) illustrates the categorized power loss distribution of conduction, passive, and switching for five HV-LV switch combinations integrated within the converter. The data, obtained through time-domain simulations with realistic switching dynamics and parasitic modelling, highlights the thermal and electrical implications of device pairing. Variant 1 achieves the most favorable performance, exhibiting the lowest total power loss (~78 W) due to well-balanced conduction and passive losses, alongside minimal switching overhead. Variants 2 and 3 also maintain efficient profiles, with comparable distribution patterns. In contrast, Variants 4 and 5 incur significantly higher total losses, most notably, Variant 5 reaches ~136 W, primarily driven by excessive conduction and passive dissipation.

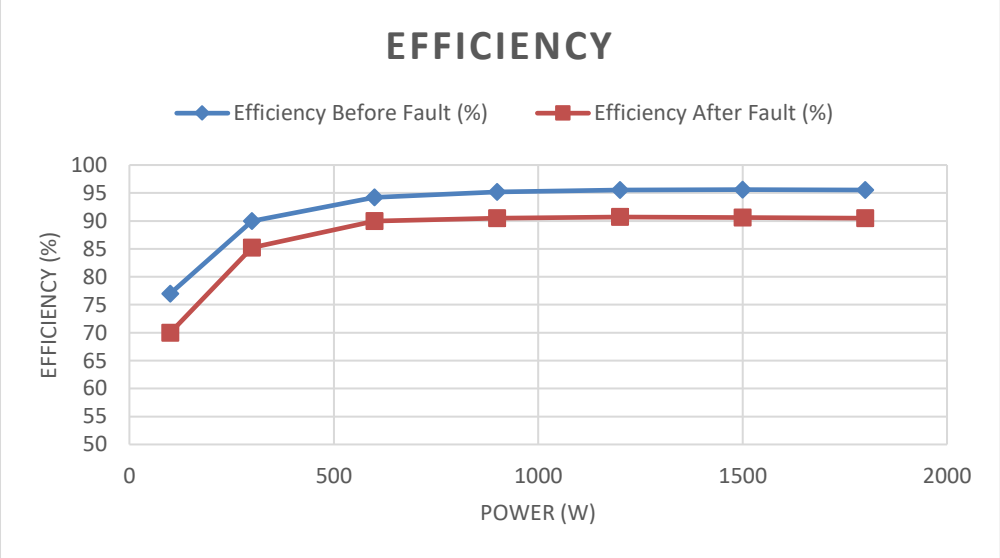

Figure 9: Load-dependent efficiency performance of variant 1 in stand-alone fault-tolerant LLC converter with VDR under pre- and post-fault conditions

Figure 9 presents the efficiency profile of Variant 1, evaluated in a standalone fault-tolerant LLC converter architecture featuring a VDR, specifically designed for safety-critical applications. The analysis spans a wide load range from 100 W to 1800 W, comparing performance in both nominal and fault-induced operating states. Variant 1 was selected from a set of optimized HV-LV switch combinations based on its superior thermal characteristics and minimized total power losses. The converter achieves a peak efficiency of approximately 96% under nominal conditions, demonstrating excellent power conversion performance. Following a representative fault event, the system sustains operational continuity with only a modest efficiency reduction, stabilizing around 91% at higher load levels. These results validate the capability of the proposed standalone fault-tolerant LLC with VDR to maintain high efficiency and uninterrupted functionality under fault scenarios, reinforcing its suitability for automotive and other safety-critical domains.

Table 6: Comparison between the stand-alone fault-tolerant LLC with VDR and other HV/LV DCDC converters

Ref.	Topology	Specification of the converter						
		Input Voltage (V)	Output Voltage (V)	Power (kW)	Peak η (%)	Full-load η (%)	Power Density (kW/L)	Switching Frequency (kHz)
[6]	PSFB	235 ~ 431	11.5 ~15	2	93.5	93	0.94	200
[7]	PSFB	300 ~ 400	12 ~16	0.72	93.5	90	-	100
[8]	LLC	220 ~ 440	6.5 ~16	2.5	93.2	92	1.17	90 ~ 200
[9]	LLC	330V~410	14	2.5	95	93	1	250
Fault-Tolerant LLC with VDR	*LLC*	*250 ~ 450*	*12*	*1.8*	*96*	*95.5 (pre-fault) 90.5 (post-fault)*	-	*97 ~ 340*

Table 7: Comparison between the stand-alone fault-tolerant LLC with VDR and other fail-operational topologies

Topology	LCC [10]	LLC + Recon. Rect. [11]	LLC with adj. n [12]	*Fault-Tolerant LLC with VDR*
Resonant Capacitors	2	1	1	*1*
Resonant Inductors	1	1	1	*1*
Limit Lm ?	no	yes		
Topology Arrangement	FB @ primary Current doubler @ secondary	FB @ primary and secondary		
FET Count	6	6	8	*10*
Diode Count	0	4	6	*0*
Capacitors	0	2	0	*0*
Gain Range	-	-	0.15 - 1.15	0.856 - 1.540
Control	PS + FM	FM	PS	*FM*
Peak Efficiency	95.3 %	97.6 %	97.5 %	*96 %*
Soft Switching	ZVS for partial range, ZCS	ZVS	ZVS and ZCS for partial range	*ZVS ZCS*
Special Features	Improved light load regulation1	*Preferred for wide input voltage range applications, + fail-operational mechanism*		

5 Summary and Outlook

This work has presented a standalone fault-tolerant LLC converter architecture integrated with a VDR, tailored for high-reliability applications such as auxiliary power supplies in Level 4/5 autonomous EVs. Distinguished by its reduced component count and structural simplicity, the topology offers a compact, efficient alternative to more complex fail-operational converter systems. Through extensive simulation studies, the converter demonstrated stable 12 V output regulation under both nominal and post-fault conditions across a wide input voltage range. The system incorporates a dynamic fault management mechanism, transitioning from FB to HB operation during fault events. This approach eliminates the need for auxiliary batteries or redundant converter paths, significantly enhancing system availability while reducing hardware overhead.

Notably, the topology ensures soft-switching on both primary and secondary sides throughout the entire operational range, improving efficiency and reducing switching stress. Peak efficiency reached approximately 95%, while post-fault operation-maintained efficiency above 90%, validating the converter's suitability for stringent energy and thermal constraints in automotive systems. Beyond the automotive domain, the robust nature of this fail-operational LLC with VDR architecture positions it as a promising solution for other safety-critical sectors such as aerospace, medical devices, and satellite systems where uninterrupted power delivery and system resilience are non-negotiable.

References

[1] H. K. Bai et al., "Charging Electric Vehicle Batteries: Wired and Wireless Power Transfer: Exploring EV charging technologies," in IEEE Power Electronics Magazine, vol. 9, no. 2, pp. 14-29, June 2022, doi: 10.1109/MPEL.2022.3173543.

[2] I. Aghabali, J. Bauman, P. J. Kollmeyer, Y. Wang, B. Bilgin and A. Emadi, "800-V Electric Vehicle Powertrains: Review and Analysis of Benefits, Challenges, and Future Trends," in IEEE Transactions on Transportation Electrification, vol. 7, no. 3, pp. 927-948, Sept. 2021, doi: 10.1109/TTE.2020.3044938.

[3] G. A. Mudiyanselage, N. Keshmiri and A. Emadi, "A Review of DC-DC Resonant Converter Topologies and Control Techniques for Electric Vehicle Applications," in IEEE Open Journal of Power Electronics, vol. 4, pp. 945-964, 2023, doi: 10.1109/OJPEL.2023.3331180.

[4] M. Pashaei, M. Hasanisadi and F. Tahami, "Comprehensive Conducted Emission Analysis of the Three-Phase

and Single-Phase LLC Resonant Converters for EV Application," in IEEE Transactions on Electromagnetic Compatibility, vol. 65, no. 5, pp. 1556-1564, Oct. 2023, doi: 10.1109/TEMC.2023.3280362.

[5] X. Zhou et al., "A High Efficiency High Power-Density LLC DC-DC Converter for Electric Vehicles (EVs) On-Board Low Voltage DC-DC Converter (LDC) Application," 2020 IEEE Applied Power Electronics Conference and Exposition (APEC), New Orleans, LA, USA, 2020, pp. 1339-1346, doi: 10.1109/APEC39645.2020.9124278.

[6] Djilali Hamza, Majid Pahlevaninezhad, and Praveen K. Jain, “Implementation of a novel digital active EMI technique in a DSP based dc–dc digital controller used in electric vehicle (EV),” IEEE Transactions on Power Electronics, vol. 28, no. 7, pp. 3126-3137, Jul. 2013.

[7] Ruoyu Hou and Ali Emadi, “A primary full-integrated active filter auxiliary power module in electrified vehicles with single-phase onboard chargers,” IEEE Transactions on Power Electronics, vol. 32, no. 11, pp. 8393-8405, Nov. 2017.

[8] Chen Duan, Hua Bai, Wei Guo and Zhong Nie, “Design of a 2.5-kW 400/12V high-efficiency dc/dc converter using a novel synchronous rectification control for electric vehicles,” IEEE Transactions on Transportation Electrification, vol. 1, no. 1, pp. 106-114, Jun. 2015.

[9] Gang Yang, Patrick Dubus and Daniel Sadarnac, “Double-phase high efficiency, wide load range high-voltage/low-voltage LLC dc/dc converter for electric/hybrid vehicles,” IEEE Transactions on Power Electronics, vol. 30, no. 4, pp. 1876-1886, Apr. 2015.

[10] Y. Chen, J. Xu, Y. Gao, L. Lin, J. Cao, and H. Ma, “Analysis and design of phase-shift pulse-frequency-modulated full-bridge LCC resonant converter,” IEEE Trans. Ind. Electron., vol. 67, no. 2, pp. 1092–1102, Feb. 2020.

[11] X. Tang, Y. Xing, H. Wu, and J. Zhao, “An improved LLC resonant converter with reconfigurable hybrid voltage multiplier and PWM-Plus-PFM hybrid control for wide output range applications,” IEEE Trans. Power Electron., vol. 35, no. 1, pp. 185–197, Jan. 2020.

[12] D. Shu and H. Wang, “An ultrawide output range LLC resonant converter based on adjustable turns ratio transformer and reconfigurable bridge,” IEEE Trans. Ind. Electron., vol. 68, no. 8, pp. 7115–7124, Aug. 2021

[13] L. Costa, G. Buticchi and M. Liserre, "A Fault-Tolerant Series-Resonant DC–DC Converter," in IEEE Transactions on Power Electronics, vol. 32, no. 2, pp. 900-905, Feb. 2017, doi: 10.1109/TPEL.2016.2585668.

[14] A. M. Prince and A. Ayad, "Analysis of Fault-Tolerant and Fully Redundant HV/LV DC-DC Converters for Battery Electric Vehicles," 2023 25th European Conference on Power Electronics and Applications (EPE'23 ECCE Europe), Aalborg, Denmark, 2023, pp. 1-9, doi: 10.23919/EPE23ECCEEurope58414.2023.10264479.

[15] Verband der Automobilindustrie e. V. (VDA), VDA Recommendation 450: Electrical Power Supply System regarding Automated Driving in the Context of ISO 26262, English version, April 2023.

Presenter Biography

Aswathy M. Prince is a PhD candidate in the Technology & Innovation Department of Schaeffler AG, Regensburg, Germany, researching fail-operational DC-DC converters for electrified transportation. She is also a PhD student at the Technical University of Munich (TUM). She holds a Master of Science in Electrical Engineering and Information Technology from Hochschule Wismar, Germany (2023), a Master’s in Power Electronics and Drives from Kerala Technological University, India (2017), and a Bachelor’s in Electrical Engineering from MG University, India (2015). Aswathy specializes in high-efficiency, fail-operational power electronics converters for automotive applications.